

Christoph Holst*, Tomislav Medić, and Heiner Kuhlmann

Dealing with systematic laser scanner errors due to misalignment at area-based deformation analyses

<https://doi.org/10.1515/jag-2017-0044>

Received December 21, 2017; accepted February 13, 2018

Abstract: The ability to acquire rapid, dense and high quality 3D data has made terrestrial laser scanners (TLS) a desirable instrument for tasks demanding a high geometrical accuracy, such as geodetic deformation analyses. However, TLS measurements are influenced by systematic errors due to internal misalignments of the instrument. The resulting errors in the point cloud might exceed the magnitude of random errors. Hence, it is important to assure that the deformation analysis is not biased by these influences. In this study, we propose and evaluate several strategies for reducing the effect of TLS misalignments on deformation analyses. The strategies are based on the bundled in-situ self-calibration and on the exploitation of two-face measurements. The strategies are verified analyzing the deformation of the Onsala Space Observatory's radio telescope's main reflector. It is demonstrated that either two-face measurements as well as the in-situ calibration of the laser scanner in a bundle adjustment improve the results of deformation analysis. The best solution is gained by a combination of both strategies.

Keywords: terrestrial laser scanner, misalignments, area-based deformation analysis, self-calibration, two-face measurements, parameter estimation, sensitivity analysis

1 Motivation

Regardless the tremendous efforts of manufacturers, terrestrial laser scanners (TLS) are not geometrically perfect instruments. Hence, they are subjected to a comprehensive factory calibration after assembly. Due to different factors, such as long term utilization and suffered stress, the internal geometry of the device can be compromised so

***Corresponding author: Christoph Holst**, Institute of Geodesy and Geoinformation, University of Bonn, Nußallee 17, 53115, Bonn, Germany, e-mail: c.holst@igg.uni-bonn.de

Tomislav Medić, Heiner Kuhlmann, Institute of Geodesy and Geoinformation, University of Bonn, Nußallee 17, 53115, Bonn, Germany, e-mails: t.medic@igg.uni-bonn.de, heiner.kuhlmann@uni-bonn.de

that the factory calibration is not valid anymore. The resulting mechanical misalignments are, e. g., the collimation axis error, trunnion axis error, vertical index offset and zero offset, to name the most relevant ones [16, 18, 25]. These systematic errors misplace all points in the point cloud to some extent. That misplacement can significantly influence the deformation analysis [10]:

- The geometry of the object might be estimated inaccurately. This might lead to falsely detected shape deformations.
- The position and orientation of the object might be estimated inaccurately. This might lead to falsely detected rigid body movements.

In both cases, the impact of the laser scanner's misalignments on the deformation analysis can be reduced either by (i) calibrating the laser scanner previous to its measurements or by (ii) using appropriate measurements strategies that reduce systematic measurement errors in-situ. Possibility (i) is not focused in this study since a specialized facility using a carefully designed network geometry is needed. Instead, we discuss the possibility (ii) in order to present effective strategies that anyone can use at laser scanner-based deformation analyses without the need for special facilities. Consequently, we answer the questions:

- What are possible in-situ strategies to deal with the laser scanner misalignment at area-based deformation analyses and
- what are their advantages and disadvantages?

One of these strategies can simply be to scan only from one station with equal orientation of the laser scanner in each measurement epoch. In this case, the errors due to misalignments impact the point cloud in each epoch similarly so that they might not affect the deformation analysis between two epochs. However, this strategy is only feasible in special cases:

- (i) The object's absolute geometry of each epoch is not of interest, i. e., only the relative changes of the geometry between two epochs are of interest,
- (ii) the absolute position and orientation of the object is not of interest,

- (iii) one laser scanner station is enough to acquire the complete object and
- (iv) the time between the epochs is reasonably short and the atmospheric conditions are similar so that the calibration parameters of the TLS can be considered to be stable.

An example satisfying all these requirements could be the high-frequency monitoring of a bridge that oscillates due to traffic using a profile laser scanner.

Commonly, these requirements cannot be met. Hence, other – more general – strategies need to be focused. Yet, in the current literature, there is no overview and detailed evaluation of strategies that might be applicable. Thus, we compare five strategies regarding their ability to deal with systematic laser scanner errors due to misalignment at area-based deformation analyses:

- Strategy 1: In-situ calibration of the laser scanner estimating a unique set of calibration parameters for each scanner station individually. As suggested by [6], we name the parameters estimated this way local calibration parameters and this strategy local calibration.
- Strategy 2: In-situ calibration of the laser scanner in a bundle adjustment using several scans. This is named global calibration from now on – as suggested in [6] – since the calibration parameters are estimated uniquely for one measurement campaign.
- Strategy 3: Scanning the object in two cycles so that each part is sampled in face 1 as well as in face 2. Here, no calibration is performed.
- Strategies 4 and 5: Local or global calibration using two-face measurements.

Strategy 1 has already been used for the deformation analysis of a radio telescope [7, 8]. Strategy 2 has its origin in the laser scanner self-calibration: Here, laser scans are performed from different stations so that the subsequent network adjustment helps to estimate a single set of calibration parameters [18, 17, 1, 19].

Strategies 3–5 exploit the fact that most of the errors due to laser scanner misalignments are two-face sensitive [21]: Hence, using two-face measurements upgrades the ability to estimate calibration parameters in a laser scanner self-calibration as also examined by [19, 21, 22].

Contrary to the literature focused on laser scanner self-calibration, we do not try to estimate unbiased and minimally correlated calibration parameters. Consequently, not all of the calibration parameters that potentially exist in the laser scanner might be predictable unbiasedly or predictable at all. If we also pursued this objective, we would need to improve the scanning configura-

tion by also sampling targets or other additionally placed objects. This strategy has been tracked by [2, 3].

On the contrary, we solely aim at increasing the accuracy of the estimated parameters describing the shape, position and orientation of the scanned object by minimizing the systematic errors in the point cloud due to laser scanner misalignment. The self-calibration of the laser scanner or the usage of two-face measurements are just methods assisting in this aim. The results of this study are important for geodetic deformation analyses and likewise for reverse engineering, dimensional quality control and as-built modelling.

2 Systematic errors due to misalignment of laser scanner

In general, a laser scanner samples the surrounding surface by a large number m of scan points that are based on measuring horizontal angles φ_j , vertical angles θ_j and slope distances r_j leading to Cartesian coordinates

$$\mathbf{x}_j = \begin{bmatrix} x_j \\ y_j \\ z_j \end{bmatrix} = \begin{bmatrix} (r_j + \Delta r_j) \cdot \sin(\theta_j + \Delta\theta_j) \cdot \sin(\varphi_j + \Delta\varphi_j) \\ (r_j + \Delta r_j) \cdot \sin(\theta_j + \Delta\theta_j) \cdot \cos(\varphi_j + \Delta\varphi_j) \\ (r_j + \Delta r_j) \cdot \cos(\theta_j + \Delta\theta_j) \end{bmatrix}_j \quad (1)$$

where $j = 1, \dots, m$. Each Cartesian coordinate might be misplaced to some extent Δr_j , $\Delta\varphi_j$ and $\Delta\theta_j$ due to random errors v_{r_j} , v_{φ_j} and v_{θ_j} and due to 18 calibration parameters x_2, x_{10}, \dots as attested by [21] for panoramic laser scanners.

From now on, we want to focus on the specific laser scanner we used for the case study presented in Sec. 3: Leica Scan Station P20. For this TLS, the 18 calibration parameters proposed by [21] can be reduced to only 11 relevant ones following [19]:

$$\Delta r_j = x_2 \sin(\theta_j) + x_{10} + v_{r_j}, \quad (2)$$

$$\Delta\varphi_j = \frac{x_{1z}}{r_j \tan \theta_j} + \frac{x_3}{r_j \sin \theta_j} + \frac{x_{5z-7}}{\tan \theta_j} + \frac{2x_6}{\sin \theta_j} + \frac{x_{1n}}{r_j} + v_{\varphi_j}, \quad (3)$$

$$\Delta\theta_j = \frac{x_{1n+2} \cos \theta_j}{r_j} + x_4 + x_{5n} \cos \theta_j - \frac{x_{1z} \sin \theta_j}{r_j} - x_{5z} \sin(\theta_j) + v_{\theta_j}. \quad (4)$$

Consequently, the calibration parameters $\tilde{\mathbf{p}}_{calib}$

$$\tilde{\mathbf{p}}_{calib} = [x_2, x_{10}, x_{1z}, x_3, x_{5z-7}, x_6, x_{1n}, x_{1n+2}, x_4, x_{5n}, x_{5z}]^T \quad (5)$$

are needed for modelling the true beam deflection and distance measurement of each laser scan point using Eq. (1).

3 Case study: Deformation analysis of radio telescope

The present study is focused on one specific example: The deformation analysis of the Onsala Space Observatory (OSO) 20-m radio telescope that is used for Very Long Baseline Interferometry (VLBI) measurements. VLBI measurements employ pairs of radio telescopes to simultaneously observe signals from quasi stellar objects for determining the difference in signal arrival times. The parameters of the baseline between the radio telescopes can then be estimated from the time delay which also depends on the signal paths within the optics of the radio telescopes [4].

Hence, changes in focal length of the main reflector or local deformations of the reflector's surface directly lead to biased signal paths and, thus, biased baseline estimates [26, 23]. Consequently, both geometric properties should be known very accurately. As they might vary due to gravitation, they should be estimated w.r.t. the elevation angle of the radio telescope leading to an elevation-dependent deformation.

A detailed introduction and motivation of this deformation analysis and also the complete explanations regarding the measurement concept and the data processing can be found in [9]. Here, only the most relevant information regarding the measurement concept, the estimation of the deformation parameters and preliminary results of the deformation analysis are given.

3.1 Measurement concept

The scans were performed at the telescope's elevation angles of 85 deg, 75 deg, 60 deg, 45 deg, 30 deg, 15 deg and 5 deg. At each elevation angle, two scan cycles were collected: In cycle 1, the scanner rotated horizontally from 0 deg to 180 deg and in cycle 2, from 180 deg to 360 deg. Consequently, each part of the main reflector is scanned twice, once in face 1 and once in face 2. This was done to account for systematic laser scanner errors due to misalignment. The relevance of this double scanning will be shown within this study. Each scan consists of about 570 million points but the point cloud is reduced to a regular point spacing with about 2 million points. This is further discussed in [8].

The support holding the TLS has been designed and manufactured particularly for laser scanners sampling radio telescopes with an upside-down orientation (Fig. 1). It consists of a bracket being attached to the radio telescope's beam and a flexible spherical hinge. During the rotation of the telescope, the hinge was unconstrained while during measurements, a pneumatic break held the scanner in a vertical position. Hence, the laser scanner was always oriented upside-down, independent of the telescope's elevation angle. However, as was found out in the data processing [9], the spherical hinge moved during the scans of 85 deg, 75 deg and 60 deg in cycle 1 so that these scans are disregarded in the further analyses whenever possible (see Sec. 4).

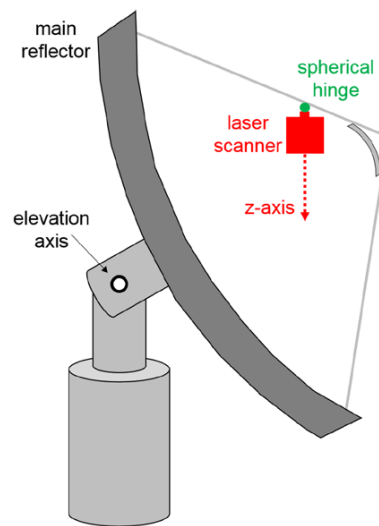


Figure 1: Sketch of the measurement configuration including radio telescope and mounting of the laser scanner.

For deformation analysis, this measurement concept means:

- There are seven epochs, i. e., each elevation angle defines a new epoch.
- We know that, for each epoch, the focal length decreased and that the object moved. Hence, the object deforms in sense of a shape deformation as well as a rigid body movement.
- The measurement configuration varied noticeably between each epoch: While the TLS saw the vertex of the radio telescope at 85 deg elevation angle approximately in direction of its local zenith, it saw the vertex at 5 deg elevation angle approximately in direction of its local horizon.

It is worth noting that the upside-down orientation of the laser scanner is not a common measurement setup. Terrestrial laser scanners are never calibrated this way. Thus, it is questionable if eventual previously estimated calibration parameters would be applicable due to the altered influence of the gravitational force on the instrument. Therefore, the strategies discussed herein could be advantageous even if the scanner was previously calibrated.

3.2 Estimation of deformation parameters

The main reflector consists of 120 solid panels forming the shape of a rotational paraboloid (see also Fig. 3). Hence, the measured point clouds of $j = 1, \dots, m$ sampling points can be parameterized by the functional model of rotational paraboloid. A rotational paraboloid can be described only by one shape parameter, i. e., the focal length f , if it is positioned in its normal form where its rotation axis equals the Z -axis of the coordinate system $[X, Y, Z]$:

$$\frac{X_j^2 + Y_j^2}{4 \cdot f} - Z_j = 0. \quad (6)$$

This is not the case since the main reflector is scanned in the laser scanner's local coordinate system $[x, y, z]$, so that the paraboloid needs to be transformed by

$$\mathbf{X}_j = \begin{bmatrix} X_j \\ Y_j \\ Z_j \end{bmatrix} = \mathbf{R}_y(\phi_y) \cdot \mathbf{R}_x(\phi_x) \cdot \mathbf{x}_j + \mathbf{X}_v \quad (7)$$

where \mathbf{R}_x and \mathbf{R}_y are the rotation matrices around the x - and y - axis and \mathbf{X}_v the translation vector. Consequently, the parameters \mathbf{p}_{obj} describing the rotational paraboloid inside the laser scanner's coordinate system equal

$$\mathbf{p}_{obj} = [X_v, Y_v, Z_v, \phi_x, \phi_y, f]^T. \quad (8)$$

For estimating the parameters \mathbf{p}_{obj} , the original polar measurements of the TLS r_j , φ_j and θ_j are integrated in Eq. (1–7). For the stochastic model Σ_{ll} , $\sigma_\varphi = \sigma_\theta = 2.5$ mgon are chosen corresponding to the manufacturer's specifications of the Leica Scan Station P20 [15]. For the distance r_j , a standard deviation of $\sigma_r = 1.5$ mm is chosen [9]. As usual, the observations are assumed to be uncorrelated and Gaussian distributed, which is – in general – an oversimplification of the reality [12, 13, 14].

The parameters are estimated using the general case of adjustment [20]: The residuals $\hat{\mathbf{v}}$ representing the errors between observations \mathbf{l} and adjusted observations $\hat{\mathbf{l}}$ are minimized following the theoretical target function $\mathbf{v}^T \Sigma_{ll}^{-1} \mathbf{v}$ [20, 28].

As results, we discuss the estimated parameters $\hat{\mathbf{p}}$ and the estimated post-fit residuals $\hat{\mathbf{v}}$. The latter ones indicate the success at minimizing systematic errors since we expect the residuals to be Gaussian distributed with zero mean due to the high precision of the telescope surface of 0.14 mm ... 0.2 mm [11]. To recognize even small systematic errors in the post-fit residuals, we further increase their signal-to-noise ratio by averaging them panel-wise leading to 120 averaged residuals.

3.3 Results not considering misalignment of laser scanner

If the laser scanner misalignments are not considered in the deformation analysis, only the previously named object parameters \mathbf{p}_{obj} are estimated based on laser scans in one cycle:

$$\mathbf{p}_{e,c} = \mathbf{p}_{obj}(e, c)_{[6 \times 1]}. \quad (9)$$

This leads to a separate parameter vector $\mathbf{p}_{e,c}$ for each telescope's elevation angle e and measurement cycle c of size $[6 \times 1]$. Hence, these parameters are estimated fourteen times (seven elevation angles in two cycles).

Fig. 2 depicts the corresponding panel-wise averaged residuals for all seven elevation angles e combined, but split to cycle 1 (red) and cycle 2 (green) measurements. Fig. 3 depicts the raw – non-averaged – residuals for an elevation angle of 45 deg, also split to cycle 1 (top) and cycle 2 (bottom). Both figures indicate, amongst others, two aspects: (1) There are systematic errors included in the point cloud. (2) These errors are two-face sensitive, at least to a large amount. This can be seen since the areal bias in residuals is mirrored for cycle 1 and cycle 2 meaning that the sign of the errors changes between face 1 and face 2.

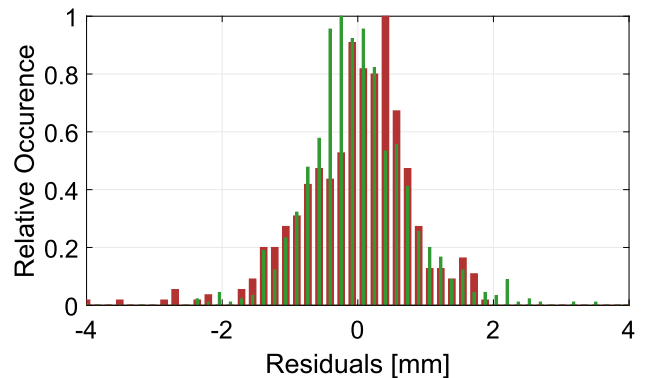


Figure 2: Not considering the misalignment of the laser scanner – Histogram of the panel-wise averaged residuals for cycle 1 (red) and cycle 2 (green).

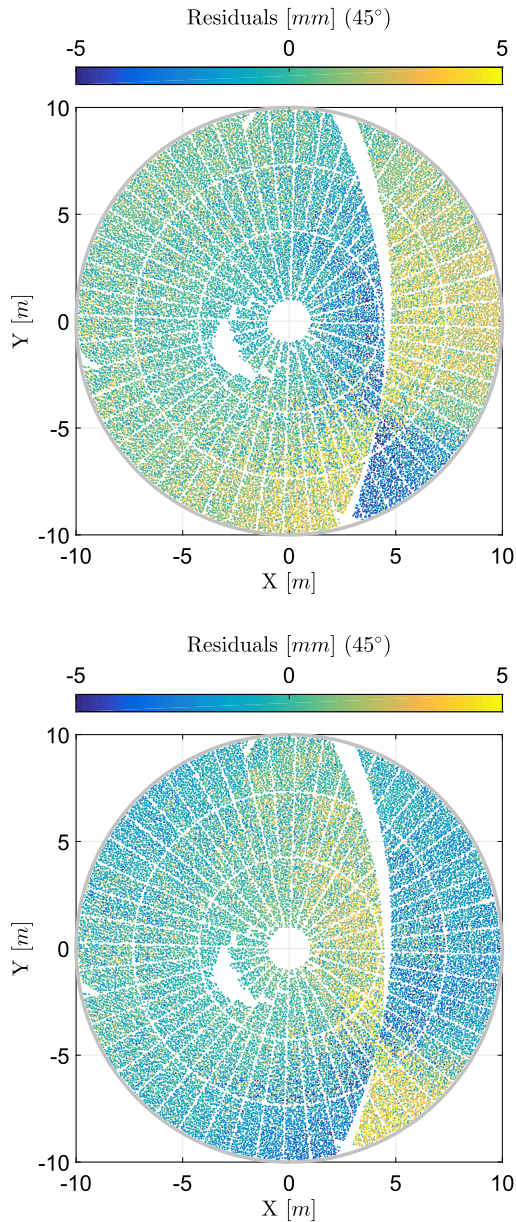


Figure 3: Top: Residuals of the deformation analysis at an elevation angle of 45 deg at cycle 1; Bottom: Corresponding residuals at cycle 2; The 120 panels are visible by the regular gaps in the point cloud. Modified from [9].

4 Proposing strategies for dealing with systematic errors

For dealing with the systematic measurement errors due to laser scanner misalignments, we set up several strategies. Each of these strategies will be motivated by its idea and its mathematical realization will be derived.

4.1 Idea of strategies

Strategy 1: Local calibration

The calibration parameters describing the misalignments are known following Eq. (5). Consequently, all calibration parameters that are predictable based on the given configuration are estimated along with the object parameters so that they absorb the systematic trend in the residuals. This is done for each elevation angle separately. Only the measurements of one cycle or scan, respectively, are necessary for this strategy.

Strategy 2: Global calibration

Strategy 1 estimates a new set of calibration parameters at each elevation angle although the corresponding error sources are expected to stay constant for all elevation angles. Strategy 2 deviates from this by estimating all calibration parameters only once in a bundle adjustment. By this, the different measurement configurations, conditioned by the telescope's elevation angle, can support each other in estimating the calibration parameters. Again, only the measurements of one cycle are necessary – solely their processing is changed.

Strategy 3: Two-face measurements

All systematic errors listed in Eqs. (2–4) are two-face sensitive, except for x_{10} , x_{1n} and x_{5z} [21, 19]. For this Strategy 3, each part of the object is measured in two faces by scanning in two cycles. Consequently, the two-face sensitive errors are supposed to extinguish each other. Contrary to the other strategies, no in-situ calibration of the laser scanner is performed. Therefore, the mechanical construction of the laser scanner does not have to be known.

Strategy 4: Local calibration using two-face measurements

Strategy 3 integrates both faces but does not account for calibration parameters. Hence, the residuals are still degraded by systematic errors not accounted for in functional or stochastic model of the adjustment. This is changed for Strategy 4: Here, the calibration parameters are estimated along with the object parameters, analogue to Strategy 1 – but this time based on two-face measurements using two cycles as in Strategy 3.

Strategy 5: Global calibration using two-face measurements

Analogue to Strategy 2, combining all elevation angles to estimate the calibration parameters in one bundle adjust-

ment improves the measurement configuration. This time, two-face measurements are included as in Strategies 3–4. Since all elevation angles and both cycles are connected in one adjustment, single scans may be omitted. This is done in the present case since the cycle 1 measurements of the elevation angles 85 deg, 75 deg and 60 deg suffer from the unstable spherical hinge. Hence, they are not used in this Strategy 5.

4.2 Realization of adjustments

Strategy 1

The parameter vector of Eq. (8) is expanded by the calibration parameters that are defined corresponding to Eqs. (2–4):

$$\mathbf{p}_{e,c} = \begin{bmatrix} \mathbf{p}_{obj}(e, c) \\ \mathbf{p}_{calib}(e, c) \end{bmatrix}_{[13 \times 1]}. \quad (10)$$

Hence, in theory, 6 object parameters and 11 calibration parameters can be estimated for each elevation angle e and cycle c independently. However, in practice, we only estimate 13 parameters: First, the rangefinder offset x_{10} is not predictable at all without a reference distance or a specially defined configuration. Second, estimating the parameters x_2 , x_{1n} and x_{5z} leads to high parameter correlations and obvious false estimates. The measurement configuration is, thus, not sufficiently sensitive to estimate these 4 parameters. Consequently, only 7 calibration parameters are incorporated in the parameter vector

$$\mathbf{p}_{calib} = [x_{1z}, x_3, x_{5z-7}, x_6, x_{1n+2}, x_4, x_{5n}]^T \quad (11)$$

that is included in Eq. (10) instead of using all calibration parameters listed in Eq. (5). These remaining errors are all two-face sensitive.

Since we scanned the radio telescope in each elevation angle in two cycles c , the estimation of the parameters in Eq. (10) can be performed twice for each elevation angle. These two estimates are completely independent from each other.

Strategy 2

The parameter vector of Eq. (8) is stringed together for all elevation angles e_1, \dots, e_7 and expanded by the 7 calibration parameters used before leading to

$$\mathbf{p}_c = \begin{bmatrix} \mathbf{p}_{obj}(e_1, c) \\ \vdots \\ \mathbf{p}_{obj}(e_7, c) \\ \mathbf{p}_{calib}(c) \end{bmatrix}_{[49 \times 1]}. \quad (12)$$

This parameter vector can be estimated for each cycle c independently, as is the case at Strategy 1.

Strategy 3

As in the case of not accounting for laser scanner errors due to misalignment (Sec. 3), only the object parameters are estimated leading to 6 parameters per elevation angle e ,

$$\mathbf{p}_e = \mathbf{p}_{obj}(e)_{[6 \times 1]}, \quad (13)$$

combined for both cycles c .

Strategy 4

The parameter vector of Eq. (8) is expanded by the calibration parameters

$$\mathbf{p}_e = \begin{bmatrix} \mathbf{p}_{obj}(e) \\ \mathbf{p}_{calib}(e) \end{bmatrix}_{[13 \times 1]} \quad (14)$$

leading to 13 parameters per elevation angle e , combined for both cycles c . Linking both cycles allows the estimation of parameter x_2 , what is not possible in Strategies 1 and 2. However, we decided to retain the same calibration parameters in order to assure directly comparable results.

Strategy 5

The parameter vector of Eq. (8) is stringed together for all elevation angles e_1, \dots, e_7 and is expanded by the 7 calibration parameters used before leading to

$$\mathbf{p} = \begin{bmatrix} \mathbf{p}_{obj}(e_1) \\ \vdots \\ \mathbf{p}_{obj}(e_7) \\ \mathbf{p}_{calib} \end{bmatrix}_{[49 \times 1]}. \quad (15)$$

Now, these 49 parameters are estimated only once, incorporating all elevation angles e and both cycles c .

5 Evaluating strategies for dealing with systematic errors

For evaluating the proposed strategies, we compare the following measures between them:

- The raw post-fit residuals: If the calibration is successful, we expect these residuals to be unbiased, Gaussian distributed and of a magnitude that is explainable by random measurement errors solely. Thus, we assume other systematic errors influencing TLS ob-

servations, such as meteorology, measurement configuration and object properties to be of less importance. Additionally, we assume the main reflector not to be locally deformed which would also lead to biased residuals. Both assumptions are discussed in [9] in more detail. Hence, by comparing the post-fit residuals between the different strategies, we can assess the success of each strategy to reduce systematic errors.

- The panel-wise averaged residuals: They also should be unbiased and Gaussian distributed. Contrary to the raw post-fit residuals, the panel-wise averaged ones can additionally be compared directly between cycle 1 and cycle 2 measurements or between the scans of different elevation angles since one single identifiable residual exists for each panel.
- The focal length f : This parameter is of most interest for the present deformation analysis since it indicates the shape deformation that is searched. Because this parameter only describes the shape, it is datum-free.
- The translation X_v and rotation ϕ_x : They represent the transformation parameters describing parts of the rigid body movement of the main reflector. Thus, they are datum-dependent.
- The strategies sensitivities according to [27] using the estimated parameter correlations.

For the focal length and the transformation parameters, we do not know the absolute expectation values. This is usual since these represent the result of deformation analysis that is searched for. However, what we know very well is that the focal length decreases smoothly with decreasing elevation angle. Deviations from this smoothness-assumption can, therefore, be justified by systematic laser scanner errors that have not been minimized sufficiently by the corresponding strategy. For the transformation parameters, we analyse how the different strategies impact the estimates of X_v and ϕ_x . Hence, the variations of these parameters between the different strategies are investigated.

The estimated precisions are not taken into account by, e.g., a variance component analysis, when evaluating the success of each strategy. The stochastic model of the deformation analysis is overly simplified since correlations between scan points are neglected. Therefore, the precision of the estimated object and calibration parameters is too optimistic and it is mainly governed by the number of observations used to compute each solution. Conclusively, this analysis would not be statistically justified, as it was demonstrated in [12].

5.1 Post-fit residuals

Fig. 4 depicts the standard deviations of the raw post-fit residuals using each strategy. By comparing the post-fit residuals between the different strategies, we can assess the success of each strategy to reduce systematic errors in general. If it is not dealt with the laser scanner misalignments, standard deviations of about 1.8 mm appear (red dotted line: cycle 1; green dotted line: cycle 2).

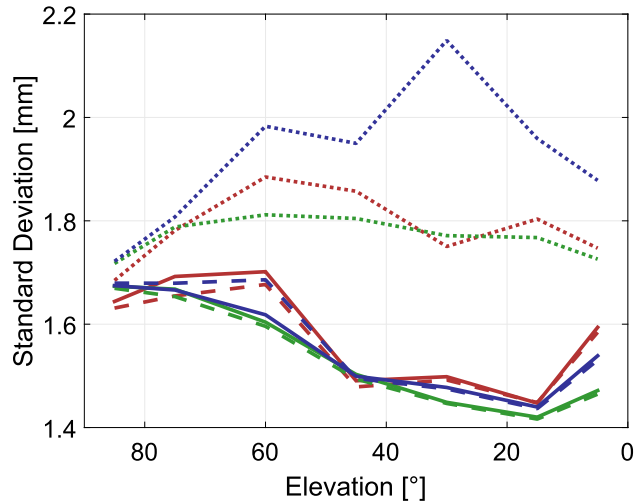


Figure 4: Standard deviation of raw post-fit residuals; No Strategy with cycle 1 (· ·) and cycle 2 (· ·), Strategy 1 with cycle 1 (— ·) and cycle 2 (· —), Strategy 2 with cycle 1 (—) and cycle 2 (—), Strategy 3 (· ·), Strategy 4 (· ·), Strategy 5 (· ·).

Strategy 1

The standard deviation of the post-fit residuals is decreased for cycle 1 as well as cycle 2 compared to not dealing with the misalignments of the laser scanner (red and green dashed lines). At the elevation angles 85 deg, 75 deg and 60 deg, the result for cycle 1 is worse since, here, the spherical hinge holding the laser scanner moved (Sec. 3). The differences between the standard deviations of cycle 1 and cycle 2 at the other elevation angles might be coincidental. In general, the systematic errors can be reduced better at the elevation angles 45 deg, 30 deg and 15 deg. This holds for all strategies.

Strategy 2

The standard deviations are similar to the ones of Strategy 1, for cycle 1 as well as cycle 2 (red and green solid lines). Consequently, the adjustment's success in reducing the systematic part in the measurement residuals is similar to the one of Strategy 1.

Strategy 3

The standard deviations are the worst for Strategy 3 (blue dotted line) – even worse than without any calibration. This is due to the fact that introducing two-face measurements makes the existence of systematic errors apparent. However, these systematic errors are not accounted for in the functional model of adjustment and, therefore, they are contained in the measurement residuals. This result shows that this type of adjustment is technically inconsistent.

Strategies 4 and 5

The standard deviations for Strategy 4 (blue dashed line) and 5 (blue solid line) are similar to those of Strategies 1 and 2. Therefore, integrating two-face measurements in the in-situ self-calibration does not improve the success of adjustment regarding the minimization of the residuals. However these values can be misleading, as it will be discussed in the following sections. At the elevation angles of 45 deg, 30 deg and 15 deg, the standard deviation is approximately an average between the cycle 1 and cycle 2 results of Strategies 1 and 2, while it deviates from that average at the other elevation angles due to the unstable spherical hinge.

5.2 Panel-wise averaged residuals

The post-fit residuals are averaged panel-wise to highlight a bias that eventually remained even after employing the proposed strategies. Tab. 1 quantifies the bias as well as the standard deviations of the panel-wise averaged residuals combined for all elevation angles: they are largest if not dealing with the laser scanner misalignment. In general, the standard deviations are noticeably smaller than the standard deviations of the raw residuals given in Fig. 4. This is expected following the law of variance propagation

Table 1: Bias and standard deviation of the panel-wise averaged residuals combined for all elevation angles split for each strategy; For Strategy “None”, 1 and 2, the values are separated for cycle 1 and cycle 2.

Strategy	Bias [mm]	Standard deviation [mm]
None	-0.03 / 0.01	0.81 / 0.76
Strategy 1	-0.01 / -0.01	0.20 / 0.22
Strategy 2	-0.01 / -0.01	0.23 / 0.26
Strategy 3	0.00	0.27
Strategy 4	0.00	0.27
Strategy 5	0.00	0.28

since these standard deviation arise out of panel-wise averaged residuals.

Strategy 1

The standard deviation is nearly quartered compared to the results without any strategy for dealing with laser scanner misalignment. However, a small bias still exists that might impact the analysis notably. For further comparison with Fig. 2, Fig. 5 depicts the histogram of the panel-wise averaged residuals: It can be seen that either the bias between both cycles as well as the standard deviation are reduced.

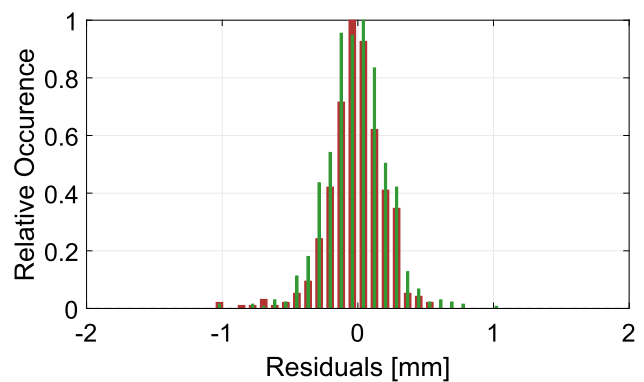


Figure 5: Strategy 1 – Histogram of the panel-wise averaged residuals for cycle 1 (red) and cycle 2 (green).

Strategy 2

The improvement compared to not dealing with the laser scanner errors is similar to the one of Strategy 1. Hence, the corresponding histogram is not displayed here.

Strategy 3

The functional model of the adjustment in Strategy 3 does not account for systematic errors of the scanner. However, including two-face measurements makes their existence prominent in the post-fit residuals of adjustment as has been seen before. Contrary, the panel-wise averaged residuals should be free of systematic errors that are two-face sensitive since cycle 1 and cycle 2 measurements are averaged on each panel. By this panel-wise averaging, we obtain a correspondence between face 1 and face 2 or cycle 1 and cycle 2, respectively, that cannot be established if we look at the raw residuals only.

As result of this averaging, there is no bias in the residuals and the standard deviation is slightly increased compared to Strategies 1 and 2. This can also be seen in the

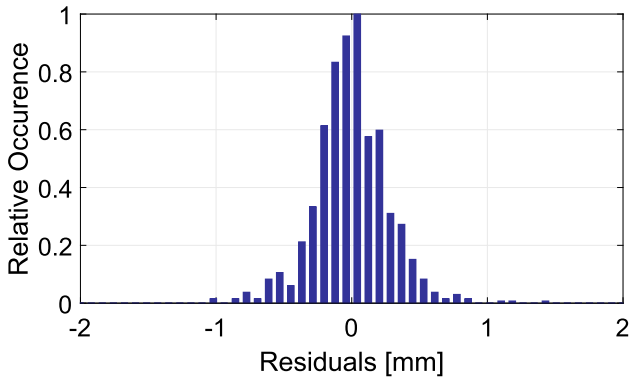


Figure 6: Strategy 3 – Histogram of the panel-wise averaged residuals combined for both cycles.

histogram in Fig. 6. The latter result can be reasoned by the fact that also the cycle 1 measurements of elevation angles 85 deg, 75 deg and 60 deg are needed in this strategy although we attest them to be degraded. In Strategies 1 and 2, they are incorporated only in the results of cycle 1 since cycle 1 and cycle 2 are processed independently.

Strategies 4 and 5

Here, the panel-wise averaged residuals are again averaged between cycle 1 and cycle 2 measurements. The bias and standard deviation are similar to the ones of Strategy 3. Thus, the corresponding histograms are not shown. Instead, Fig. 7 depicts the averaged post-fit residuals at

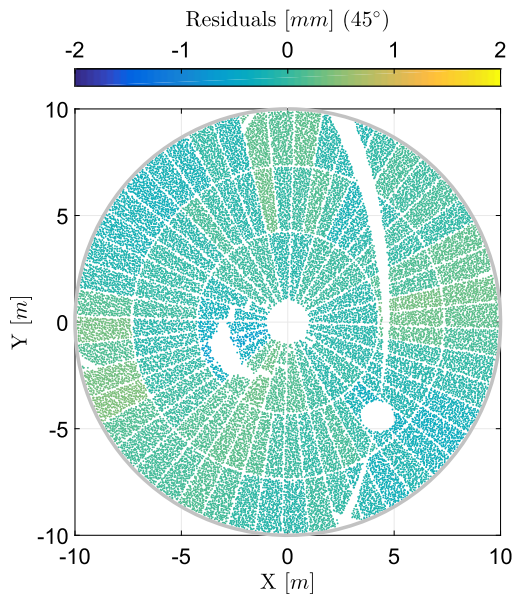


Figure 7: Panel-wise averaged residuals at an elevation angle of 45 deg using Strategy 5. Modified from [9].

45 deg elevation angle for Strategy 5. It can be seen that the bias in the residuals that is visible between cycle 1 and cycle 2 measurements in Fig. 3 vanished.

By comparing the averaged residuals between different panels on the main reflector, variations of about -0.5 mm to 0.5 mm can still be observed, where the residuals of neighbored panels show similar behavior. This result can be explained by not modelled systematic effects of the TLS, as well as possible other systematic effects influencing the reflectorless distance measurements. We do not reason these variations with areal deformations of the reflector since the magnitude and sign of these residuals vary randomly between different angles as written in [9].

5.3 Estimated focal lengths

Fig. 8 depicts the focal length estimates that are of main interest for the present deformation analysis. If it is not dealt with the laser scanner misalignments (red and green dotted lines), the estimated focal lengths deviate significantly from the assumption of a smooth elevation-dependent decrease.

In Fig. 8, we do not include error bars since they are too optimistic due to the neglected correlations in the stochastic model, as mentioned before. The estimated precisions have an unrealistic magnitude of about 0.05 mm or less. These small values strongly depend on the number of points used for estimation since every point is assumed to give one hundred percent new information.

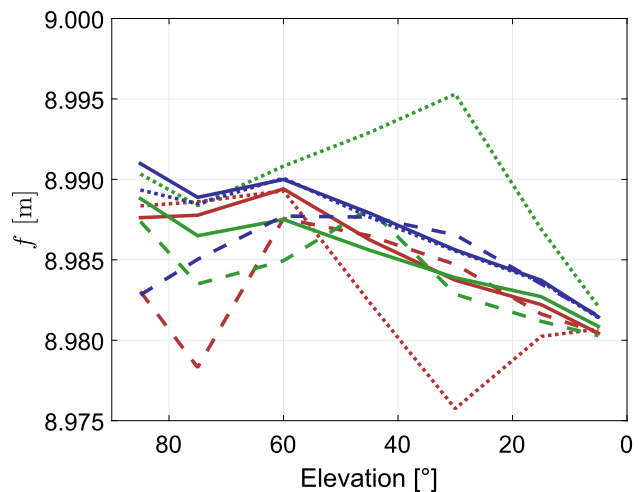


Figure 8: Estimated focal lengths; No Strategy with cycle 1 (---) and cycle 2 (---), Strategy 1 with cycle 1 (---) and cycle 2 (---), Strategy 2 with cycle 1 (---) and cycle 2 (---), Strategy 3 (---), Strategy 4 (---), Strategy 5 (---).

Strategy 1

The smoothness in the focal length change does not improve using Strategy 1 (red and green dashed lines). Additionally, the estimates for cycle 1 at 85 deg and 75 deg are not meaningful – but explainable by the missing stability of the hinge holding the laser scanner. At the other elevation angles, the smoothness is indeed increased and the differences between cycle 1 and cycle 2 are smaller but still present.

Strategy 2

The focal length estimates are noticeably smoother for Strategy 2 compared to the previous one (red and green solid lines); with the known problems for cycle 1. Consequently, the condition that the calibration parameters remain static for all elevation angles improves the focal length estimates. This supports the idea of this strategy: each elevation angle is only partially suited to estimate all calibration parameters; only a combination of all elevation angles for estimating the calibration parameters indeed improves the estimation of the shape parameter.

Strategy 3

The focal length estimates noticeably improve regarding their smoothness-assumption by using two-face measurements (blue dotted line): Only the estimates at 85 deg and 75 deg differ from this assumption – here, the degraded cycle 1 scans are responsible. In general, the focal length estimates of this strategy are an average of the results that occur for cycle 1 and cycle 2 measurements if the systematic errors are not accounted for (green and red dotted line).

Strategy 4

The estimated focal lengths do not decrease smoothly with decreasing elevation angles (blue dashed line). In fact, it even increases between 85 deg and 60 deg. Since this behaviour is not reasonable, this local calibration does not improve the deformation analysis. This can again be reasoned for the elevation angles 85 deg, 75 deg and 60 deg by the unstable spherical hinge at cycle 1 measurements that need to be included here in the data processing since all elevation angles are estimated individually as written in Eq. (14).

Strategy 5

The focal length estimates describe the smoothest decrease compared to the other strategies (blue solid line). The only deviation from this smoothness assumption is at 75 deg elevation angle. In general, the result is similar to

the one of Strategy 3 that simply uses two-face measurements for deformation analysis. The only exceptions are at 85 deg and 75 deg elevation angle since the corresponding cycle 1 measurements are omitted in Strategy 5 due to the unstable spherical hinge.

Since the decrease of the focal length is smoothed at Strategy 5 the best, the abnormal behavior at 85 deg elevation angle becomes obvious. Retrospectively, that can also be observed at other strategies. An explanation for this behavior is not at hand since the residuals of the corresponding point cloud are similar to the ones of the other elevation angles. There is, thus, no hint for unmodelled artefacts in the data.

5.4 Estimated transformation parameters

The comparison of the transformation parameter estimates is based on relative differences between the strategies, which is achieved by subtracting the average of all strategies at each elevation angle, see Figs. 9 and 10. The results without dealing with laser scanner misalignments (red and green dotted lines) deviate from this average the most, considering all elevation angles. From this, two conclusions can be drawn: First, the estimates of the transformation parameters are biased without accounting for the laser scanner misalignments. Second, this bias can be reduced using at least some of the mentioned strategies. This is evaluated in the following.

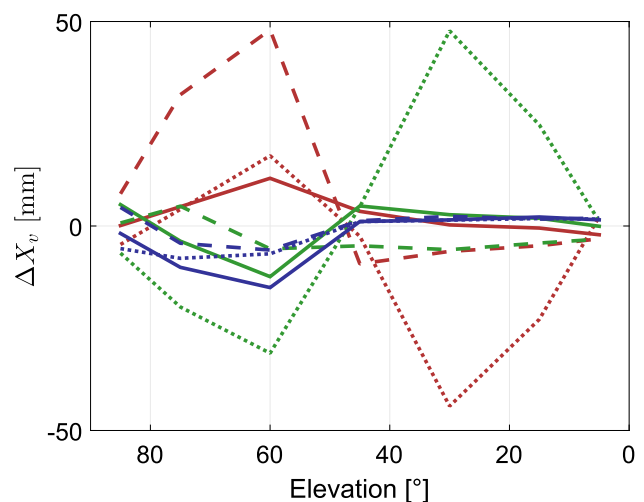


Figure 9: Estimated translations along X-axis; No Strategy with cycle 1 (- -) and cycle 2 (- -), Strategy 1 with cycle 1 (- -) and cycle 2 (- -), Strategy 2 with cycle 1 (-) and cycle 2 (-), Strategy 3 (- · -), Strategy 4 (- -), Strategy 5 (-).

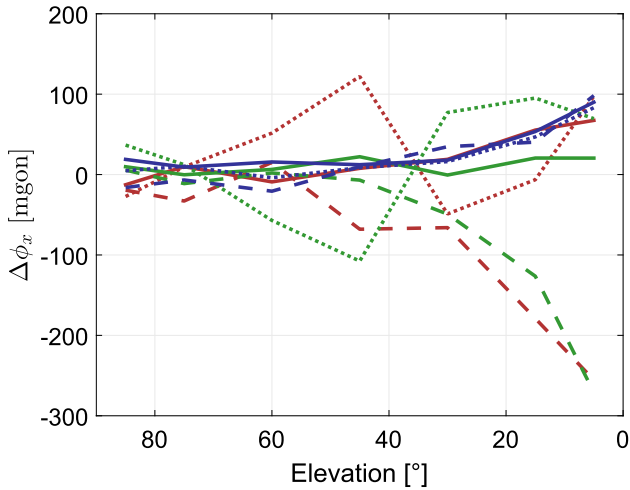


Figure 10: Estimated rotations around x -axis; No Strategy with cycle 1 (· ·) and cycle 2 (· ·), Strategy 1 with cycle 1 (— —) and cycle 2 (— —), Strategy 2 with cycle 1 (—) and cycle 2 (—), Strategy 3 (· ·), Strategy 4 (— —), Strategy 5 (—).

Strategy 1

The variation of the translation X_v is decreased for cycle 2 (green dashed line). For cycle 1, this only holds partly due to the known reasons (red dashed line). Contrary, the estimates of the rotation ϕ_x differ noticeably from those of the other strategies, up to 250 mgon. Strategy 1, thus, impacts the estimated orientation of the main reflector by a large amount.

Strategies 2 and 3

The statements regarding the focal length estimate can be recapitulated for the transformation parameters of Strategy 2 (red and green solid lines) and Strategy 3 (blue dotted line): The bias between cycle 1 and cycle 2 is smaller for Strategy 2. For Strategy 3, the transformation parameters are an average of the results as if cycle 1 and cycle 2 measurements are processed independently from each other without accounting for systematic errors (red and green dotted lines). Therefore, the estimates of the transformation parameters noticeably improve using these two strategies.

Strategies 4 and 5

The variation of the transformation parameters is again smaller compared to not dealing with the laser scanner misalignment (Strategy 4: blue dashed line; Strategy 5: blue solid line). Conclusively, Fig. 10 indicates that the strategies relying on two-face measurements show more success in reducing the bias in the estimates of the trans-

formation parameters describing the rigid body movement of the main reflector.

5.5 Sensitivity of strategies

The aim of this study is to perform a deformation analysis as unaffected from the misalignment of the laser scanner as possible. Thus, the proposed strategies should minimize the systematic errors in the point cloud due to this misalignment. Simultaneously, the strategies should not lead to large correlations between object parameters – that are of interest – and calibration parameters – that are not of primary interest. If there are large correlations between both groups, the object parameters are very sensitive regarding the ability to determine the calibration parameters unbiasedly and to determine all of them.

However, this task is hardly feasible since it relies on the scanning configuration and on the geometry of the specific object which

- is found on the job site,
- is not specially designed for the scanner calibration,
- might be unknown due to deformations.

Consequently, we investigate the sensitivity of each strategy in sense of the correlations between object parameters and calibration parameters. The correlation values analysed in this section are derived from the estimated covariance matrix of the parameters $\Sigma_{\hat{p}\hat{p}}$ by

$$K_{\hat{p}\hat{p},ij} = \frac{\Sigma_{\hat{p}\hat{p},ij}}{\sqrt{\Sigma_{\hat{p}\hat{p},ii}} \cdot \sqrt{\Sigma_{\hat{p}\hat{p},jj}}}, \quad (16)$$

with $i = 1, \dots, u$, $j = 1, \dots, u$ and u being the number of parameters. Special focus is led on the question whether two-face measurements (Strategies 3–5) or a bundle adjustment (Strategies 2 and 5) decorrelate these parameter groups.

Strategy 1

Strategy 1 is very sensitive regarding the choice of calibration parameters. Fig. 11 depicts the corresponding correlations exemplary for an elevation angle of 85 deg and 5 deg, cycle 2. Looking at both figures separately, the absolute correlations within the object parameters \mathbf{p}_{obj} (Eq. 8) and within the calibration parameters \mathbf{p}_{calib} (Eq. 11) can reach large values. Also between both groups, large absolute correlations exist. Consequently, the values of the calibration parameters and the choice of calibration parameters that are estimated impact the estimation of the object parameters and, thus, the deformation analysis.

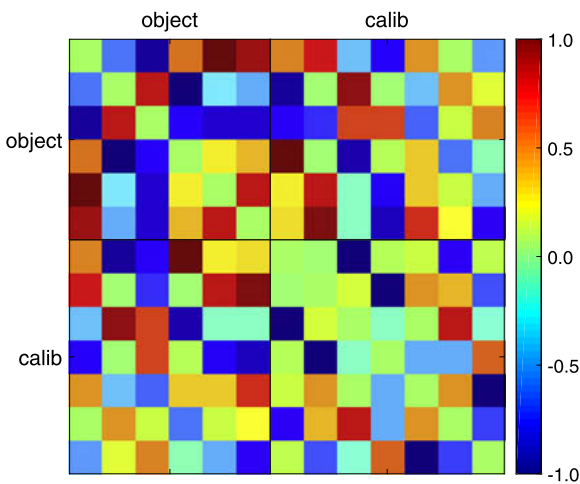
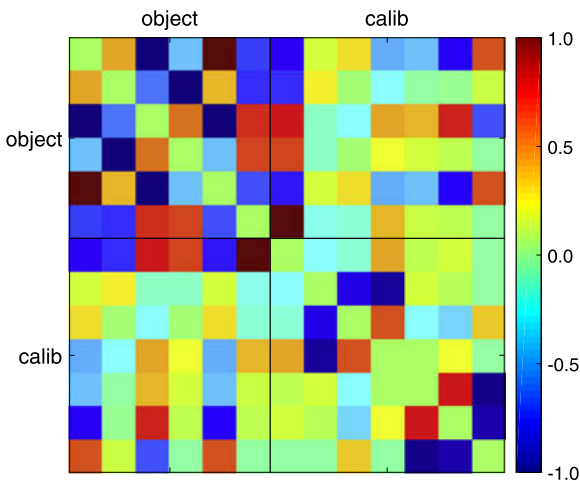


Figure 11: Strategy 1 – Correlations between estimated parameters at an elevation angle of 85 deg (top) and 5 deg (bottom), cycle 2.

Comparing both figures, differences can also be seen. This suggests that the dependencies between object parameters and calibration parameters vary between the elevation angles so that the choice of calibration parameters impacts the deformation analysis differently at each elevation angle.

Both facts help to reason the behaviour of the estimated rotation ϕ_x depicted in Fig. 10 (red and green dashed lines): The correlations between ϕ_x and the calibration parameters increase from 85 deg to 5 deg elevation angle. Thus, inaccurate estimates of the calibration parameters affect ϕ_x more at low elevation angles.

Strategy 2

Fig. 12 depicts: The number of parameters being correlated to others by a large amount decreases compared to Fig. 11. This holds for the correlations within the object param-

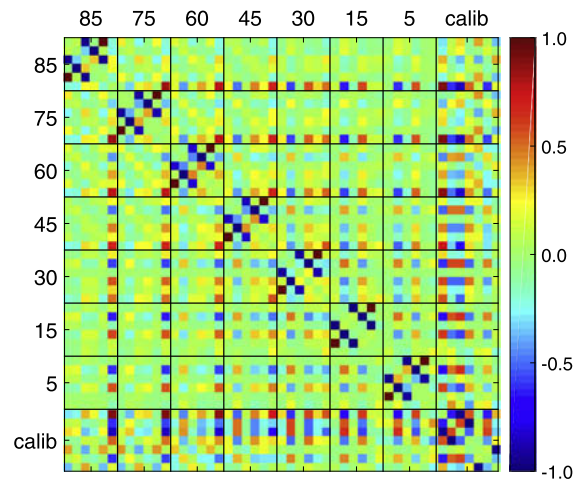


Figure 12: Strategy 2 – Correlations between all estimated object parameters at elevation angles 85 deg, ..., 5 deg (sorted as specified in Eq. (8)) and the calibration parameters (sorted as specified in Eq. (11)); cycle 2.

ters of each elevation angle as well as between the object parameters and the calibration parameters. Hence, compared to Strategy 1, Strategy 2 does not depend that much on the specific calibration parameters any more.

Simultaneously, the object parameters of different elevation angles are now correlated. Hence, they support each other. This can be highlighted by one example: The focal length estimate f at 85 deg elevation angle (6th parameter) is correlated by about 50% with the rotation around the x -axis ϕ_x at 5 deg elevation angle. Hence, configurations that are weak to determine specific calibration or object parameters are improved by others that may have been weak to determine another set of parameters.

Thus, the combination of all elevation angles in a bundle adjustment estimating one set of calibration parameters decreases the sensitivity of adjustment towards laser scanner misalignments. These results are expected based on the common knowledge about the photogrammetric bundle adjustment (e.g., [5]) and they are in accordance with the experiment described in [2]. Therefore, this Strategy 2 is less sensitive than the local calibration of Strategy 1.

Strategy 3

No calibration parameters are estimated. Hence, this Strategy 3 does not depend on the choice of calibration parameters and on the question, if the configuration of adjustment is sensitive enough to estimate a specific set of calibration parameters. The impact of the two-face sensitive parameters is reduced in any case.

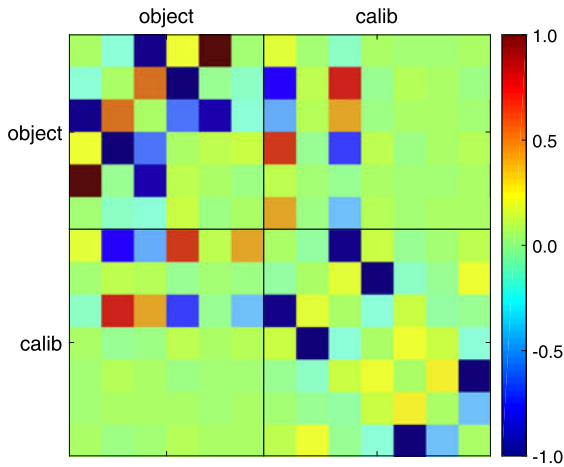


Figure 13: Strategy 4 – Correlations between estimated parameters at an elevation angle of 5 deg.

Strategy 4

Compared to Strategy 1 where the same adjustment is applied but only using one cycle, the sensitivity of the adjustment is reduced. This can be seen in Fig. 13 compared to Fig. 11 (bottom): Both figures depict the correlations at an elevation angle of 5 deg. At Strategy 4, the correlations are noticeably smaller within the object parameters, the calibration parameters as well as between both groups. This explains why the bias of the estimated rotation ϕ_x at elevation angles smaller than 45 deg does not occur at Strategy 4 while it occurs at Strategy 1. Consequently, the sensitivity of the deformation analysis regarding the laser scanner misalignments decreases at local self-calibrations if two-face measurements are included.

These results are expected based on the known influence of two-face measurements on deformation monitoring using total stations (e. g., [24]) and based on attested importance in the TLS calibration (e. g., [21]). However, to the authors' knowledge, our study presents the first application of two-face measurements in laser scanner-based deformation analyses.

Strategy 5

Fig. 14 depicts the correlations between the estimated parameters. For analysing the sensitivity of adjustment, two comparisons shall be focused. First:

- We compare the correlations between the object parameters \mathbf{p}_{obj} at 85 deg, 75 deg, 60 deg elevation angle and the calibration parameters \mathbf{p}_{calib} (bottom row of black boxes in Fig. 14, three left boxes) with
- the correlations between the object parameters \mathbf{p}_{obj} at 45 deg, 30 deg, 15 deg, 5 deg elevation angle and

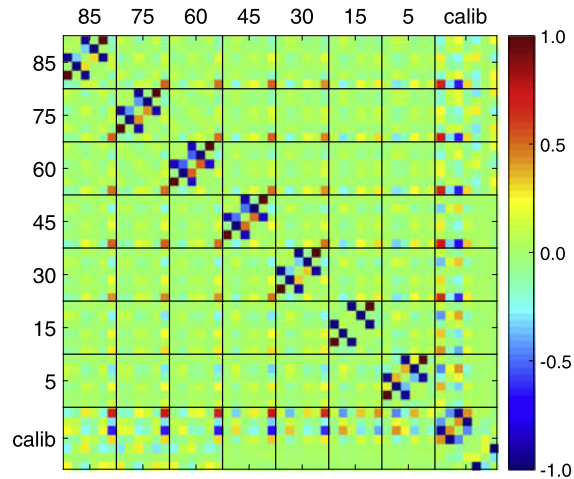


Figure 14: Strategy 5 – Correlations between all estimated object parameters at elevation angles 85 deg, ..., 5 deg (sorted as specified in Eq. 8) and the calibration parameters (sorted as specified in Eq. 11).

the calibration parameters \mathbf{p}_{calib} (bottom row of black boxes in Fig. 14, five right boxes).

At (a), only cycle 2 measurements are included due to the lack of TLS stability of the firstly scanned cycles. At (b), both cycles are included. The correlations of x_{1n+2} and x_{5n} (5th and 7th calibration parameter) to the object parameters are noticeably larger in case (a) compared to case (b). Looking at Fig. 12 of Strategy 2, it can be seen that the correlations between the object parameters and all calibration parameters increase even more if the measurements of the second cycle are completely removed from the adjustment. Thus, including two-face measurements improves the separability between object parameters and calibration parameters.

Second: We compare the correlations between the calibration parameters and the object parameters considering the different elevation angles (complete bottom row of black boxes in Fig. 14): Some correlations increase with decreasing elevation angles (e. g., the one between Y_v and x_{5z-7} , 3rd calibration parameter), some decrease (e. g., the one between f and x_{1z} , 1st calibration parameter). Consequently, the combination of the different elevation angles in one bundle adjustment improves the separability of the object parameters from the calibration parameters.

6 Discussion of results

Based on the given results, we observe that the systematic errors due to laser scanner misalignments lead to

- large and systematically distributed post-fit residuals (Sec. 5.1–5.2)
- an inaccurate estimate of the observed object's shape, i. e., the focal length (Sec. 5.3), and
- an inaccurate estimate of the object's position and orientation (Sec. 5.4).

To improve the results of deformation analyses in consideration of these troubles, five strategies are presented. These are based on self-calibration (Strategies 1–2), two-face measurements (Strategy 3) or a combination of both (Strategies 4–5). By the analyses of the previous section, we can answer the following questions regarding the ability of the strategies to reduce the bias in the residuals, in shape and transformation parameters.

6.1 Do all strategies minimize the bias in the residuals in each elevation angle?

All strategies are able to reduce the systematic part in the residuals as can be seen in Tab. 1 using the panel-wise averaged residuals. This is also depicted in Fig. 7 for Strategy 5; the results of the other Strategies 1–4 are similar.

On the contrary, when looking at the raw post-fit residuals in Fig. 4, Strategy 3 is not able to remove the systematic part: The problem of Strategy 3 is that it does not account for the laser scanner misalignments in the functional model of adjustment. Consequently, Strategy 3 is only suited to minimize the systematic in the residuals if the residuals of cycle 1 and cycle 2 measurements are averaged. In this work, we used the panel-wise averaging since the main reflector can be mechanically divided in 120 individual panels. At other objects, similar strategies could be employed if a priori knowledge about the object of interest is available.

6.2 Does a laser scanner in-situ calibration minimize the parameter bias in each elevation angle?

In-situ calibrations based only on one-face measurements are calculated in Strategies 1 and 2. For Strategy 1 (local in-situ calibration) that calibrates each laser scan separately, the question has to be answered with no: By estimating the calibration parameters along with the object parameters, the adjustment might end in parameter estimates that minimize the squared residuals the best, but that are senseless regarding deformation analysis. This might happen if the functional model of individual calibration pa-

parameter coincides with the one of the object parameters that are searched. In these cases, the laser scanner misalignments change the laser scan of the deformed object in a way that could also be explained by changes in shape, position or orientation of the object.

This dependence can, e. g., be seen for the estimated rotation parameter ϕ_x (Fig. 10): At low elevation angles, this object parameter drifts away. At the same elevation angles, the correlation of this parameter is nearly +1 with the parameter x_{1z} (vertical beam offset) and -1 with the parameter x_{5z-7} (trunnion axis error), depicted in Fig. 11 (bottom) for an elevation angle of 5 deg.

For Strategy 2 (global in-situ calibration) that calibrates all laser scans of one cycle combined in a bundle adjustment, the question has to be answered with yes. Linking all elevation angles improves the network configuration and, thus, the ability to distinguish the main reflector's shape from the systematic errors due to misalignments. This can be underlined by the decreased correlation between calibration parameters and object parameters when comparing Fig. 11 and Fig. 12.

Consequently, an in-situ calibration based on one-face measurements can be able to remove the parameter bias. As requirement, the object needs to be scanned from several stations so that these scans can be linked in a bundle adjustment estimating one set of calibration parameters. The measurement configuration between these scans has to be varied sufficiently to strengthen the support between the scans to estimate object parameters that are only correlated low to the calibration parameters.

6.3 Does two-face scanning minimize the parameter bias in each elevation angle?

Strategy 3 using two-face measurements without in-situ calibration in general leads to the same parameter estimates as Strategy 5 that additionally calibrates the laser scanner in-situ. This is redexpected since only two-face sensitive calibration parameters are estimated in Strategy 5. Consequently, in general, the question has to be answered with yes.

However, in the presented example, the equivalence of the results between Strategy 3 and 5 is not given for the elevation angles 85, 75 and 60 deg due to the corrupted cycle 1 scans. These scans can be safely removed from the deformation analysis in Strategy 5 because the calibration parameter estimates are supported by the information from the other elevation angles and automatically applied on all observations. Contrary, for Strategy 3, both cycle 1 (corrupted) and cycle 2 (uncorrupted) measurements need

to be included to reduce the influence of the scanner misalignments.

The two-face scanning is, thus, principally suited to reduce the bias in the estimated parameters. However, the corresponding estimated precisions of the parameters are still too optimistic in this Strategy 3 since the functional model does not account for the calibration parameters. E. g., the estimated precisions of the focal length are about 0.01 mm at each elevation angle for Strategy 3, while they range from 0.05 mm to 0.01 mm at different elevation angles for Strategy 5 that accounts for the calibration parameters in the functional model. Hence, there is a factor of 5 at some elevation angles between Strategies 3 and 5.

Consequently, while two-face scanning indeed minimizes the bias in the estimated parameters, it does not minimize the bias in the parameters' estimated precisions. This disagreement in precision is independent from considering correlations in the stochastic model or not.

6.4 What is the best strategy for this study?

First, two-face measurements noticeably improve the estimates of the calibration parameters and, therefore, help to reduce the misalignment errors' effect on the observations. Hence, Strategy 3, 4 and 5 yield much better results in the comparison to Strategy 1. Second, combining all epochs (main reflector's elevation angles) in one bundle adjustment improves the geometry of the network used to estimate the calibration parameters. This helps both to improve the accuracy of their estimates and to reduce correlations between calibration and object parameters. Conclusively, the combination of both ideas in Strategy 5 – global in-situ calibration and two-face measurements – yields the best results. This evaluation holds in specific for this study since some of the cycle 1 scans are corrupted due to the spherical hinge so that two-face scans are not present at each elevation angle.

In general, this favoured Strategy 5 has high requirements for scanning time and processing time. Thus, it could be considered that not every new scan might improve the measurement geometry noticeably. Hence, as update of Strategy 5, the object might be scanned only from selected stations in two cycles. The calibration parameters are calculated based on this selected information and automatically applied on all observations. In this case, attention should be placed on the selection of scanner stations that will serve for two-face scanning.

The best compromise between reducing field and computational time and achieving satisfactory results would

be scanning only the extreme elevation angles in two faces (85 and 5 deg) since these have the most different measurement geometry. This improved strategy 5 is not actually processed here due to the corrupted cycle 1 measurements at 85 deg elevation angle.

7 Transfer to deformation analyses in general

The results are now transferred to deformation analyses in general considering two-face measurements and in-situ calibrations.

7.1 Using two-face measurements

The inclusion of two-face measurements is largely applicable, regardless the individual characteristic of the specific geodetic task. The only requirement is that the used laser scanner allows measuring in both faces, which holds true for all panoramic type terrestrial laser scanners due to their assembly. The only limiting factor can be the in-built software. However, this could be overcome by a coarse rotation of the instrument, allowing cycle 1 and cycle 2 scans from a single station. The applicability of this procedure has yet to be investigated.

Generally, using two-face measurements can completely remove the influence of all two-face sensitive scanner misalignments and, therefore, improve the accuracy of estimating deformation parameters. The remaining problems are the identification and modelling of laser scanner misalignments not sensitive to two-face measurements. This might require an additional calibration of the laser scanner – either in-situ or not.

7.2 Using in-situ self-calibration

From the analysis of the different in-situ calibration strategies, the prominent conclusion is that the success of this approach strongly depends on the measurement geometry of the specific geodetic task. The more versatile the measurements during the deformation analysis are, the better is the possibility of estimating accurate TLS calibration parameters. This procedure takes advantage of the presumption that the calibration parameters do not change during one assignment. That allows all scans collected on the job scene to be bundled in one adjustment procedure with en-

hanced sensitivity regarding laser scanner misalignment detection.

There are two important prerequisites for this procedure:

- (a) the object of interest needs to be scanned from several scanner stations with altering measurement geometry between the scanner and the object and
- (b) some a priori knowledge about the deformed object geometry is needed.

In our case study, both prerequisites are fulfilled: (a) each telescope's elevation angle is measured with different measurement configuration and (b) the telescope's main reflector is designed as a rotational paraboloid. The first prerequisite is usually accomplished without any extra effort because most geodetic monitoring tasks aim at objects that are generally too big to be scanned from one scanner station. Those are for example dams, tunnels, bridges and tall raise building. The second prerequisite is also usually fulfilled because objects of interest are often man-made buildings, which can be approximated with one or more simple primitives. If not, assumptions about the object's smoothness might be incorporated to link the different point clouds together.

8 Conclusion

Insufficiently modelled terrestrial laser scanner misalignments can significantly bias the deformation analysis. This is demonstrated evaluating the elevation-dependent deformation of the OSO 20-m radio telescope's main reflector. Since the laser scanner calibration prior to engineering tasks may not always be feasible, we present different strategies to overcome the degradation of deformation analyses due to laser scanner misalignments. Our main conclusions are:

- (i) Scanning in two-faces helps since most errors due to laser scanner misalignment are two-face sensitive. By scanning all parts of the deformed object in two faces, the errors can be eliminated by averaging. This approach is easy to implement since it only requires doubled scanning time and no knowledge about the laser scanners assembly.
- (ii) Varying the scanning geometry in each epoch enables an in-situ calibration of the laser scanner based on a bundle adjustment. In this calibration, parameters not being two-face sensitive might also be estimated so that their errors are eliminated additionally. This approach is more strict compared to the previous one

since it accounts for systematic errors in the functional model of adjustment. Nevertheless, it is more difficult to implement since detailed knowledge about the laser scanner's assembly needs to exist and its success depends on the adjustment's configuration that is not easy to assess at time of scanning.

To conclude, both including two-face measurements as well as applying an in-situ calibration noticeably improve the results of deformation analyses. The final choice of optimal solution strongly depends on the individual deformation task: size and shape of deformed object, laser scanner characteristics, measurement geometry and available time for generating the solution. Therefore, the decision cannot be generalized and should be made by qualified professionals for every assignment separately.

References

- [1] M. A. Abbas, H. Setan, Z. Majid, K. M. Idris, M. F. Mohd Ariff, A. K. Chong and D. D. Lichti, The effect of datum constraints for terrestrial laser scanner self-calibration, in: *FIG Congress 2014, Kuala Lumpur, Malaysia 16–21 June 2014*, 2014.
- [2] Mohd Azwan Abbas, Derek D. Lichti, Albert K. Chong, Halim Setan, Zulkepli Majid, Chong Luh Lau, Khairulnizam M. Idris and Mohd Farid Mohd Ariff, Improvements to the accuracy of prototype ship models measurement method using terrestrial laser scanner, *Measurement* 100 (2017), 301–310.
- [3] Jacky C. K. Chow, William F. Teskey and J. W. Lovse, *In-situ Self-calibration of Terrestrial Laser Scanners and Deformation Analysis Using Both Signalized Targets and Intersection of Planes for Indoor Applications*, 1st Joint International Symposium on Deformation Monitoring (JISDM), 2011.
- [4] T. A. Clark and P. Thomsen, *Deformations in VLBI antennas*, Nasa Technical Memorandum 100696, NASA, Greenbelt, Md., Report, 1988.
- [5] W. Förstner and B. Wrobel, *Photogrammetric Computer Vision. Statistics, Geometry, Orientation and Reconstruction*, Springer International Publishing, 2016.
- [6] D. García-San-Miguel and J. L. Lerma, Geometric calibration of a terrestrial laser scanner with local additional parameters: An automatic strategy., *ISPRS J. Photogramm.* 79 (2013), 122–136.
- [7] C. Holst and H. Kuhlmann, Aiming at self-calibration of terrestrial laser scanners using only one single object and one single scan, *J. Appl. Geodesy* 8 (2014), 295–310.
- [8] C. Holst, A. Nothnagel, M. Blome, P. Becker, M. Eichborn and H. Kuhlmann, Improved area-based deformation analysis of a radio telescope's main reflector based on terrestrial laser scanning, *J. Appl. Geodesy* 9 (2015), 1–13.
- [9] C. Holst, D. Schunck, A. Nothnagel, R. Haas, L. Wennerbäck, H. Olofsson, R. Hammargren and H. Kuhlmann, Terrestrial Laser Scanner Two-Face Measurements for Analyzing the Elevation-Dependent Deformation of the Onsala Space Observatory 20-m Radio Telescope's Main Reflector in a Bundle Adjustment, *Sensors* 1833 (2017).

- [10] Christoph Holst and Heiner Kuhlmann, Challenges and Present Fields of Action at Laser Scanner Based Deformation Analyses, *J. Appl. Geodesy* 10 (2016), 17–25.
- [11] Lars E. B. Johansson, A. O. H. Olofsson and E. De Beck, *OSO 20 m Telescope Handbook*, Onsala Space Observatory, Report, 2016.
- [12] Tobias Jurek, Heiner Kuhlmann and Christoph Holst, Impact of spatial correlations on the surface estimation based on terrestrial laser scanning, *J. Appl. Geodesy* 11 (3) (2017), 143–155.
- [13] Stephanie Kauker, Christoph Holst, Volker Schwieger, Heiner Kuhlmann and Steffen Schön, Spatio-temporal Correlations of Terrestrial Laser Scanning, *Allgem. Verm. Nachr.* (2016), 170–182.
- [14] Stephanie Kauker and Volker Schwieger, A synthetic covariance matrix for monitoring by terrestrial laser scanning, *J. Appl. Geodesy* 11 (2) (2017), 77–87.
- [15] Leica Geosystems, *Leica ScanStation P20, industry's best performing ultra-high speed scanner*, www.leica-geosystems.de, Juli 2014.
- [16] D. D. Lichti, The impact of angle parameterisation on terrestrial laser scanner self-calibration, *Int. Arch. Photogramm. Remote Sens. Spat. Inf. Sci.* 38 (2009), 171–176.
- [17] D. D. Lichti, Terrestrial laser scanner self-calibration: Correlation sources and their mitigation, *ISPRS J. Photogramm.* 65 (2010), 93–102.
- [18] D. D. Lichti, J. Chow and H. Lahamy, Parameter de-correlation and model-identification in hybrid-style terrestrial laser scanner self-calibration, *ISPRS J. Photogramm.* 66 (2011), 317–326.
- [19] Tomislav Medić, Christoph Holst and Heiner Kuhlmann, Towards system calibration of panoramic laser scanners from a single station, *Sensors* 1145 (2017).
- [20] E. M. Mikhail and F. Ackermann, *Observations and least squares*, Dun-Donnelly, New York, 1976.
- [21] B. Muralikrishnan, M. Ferrucci, D. Sawyer, G. Gerner, V. Lee, C. Blackburn, S. Phillips, P. Petrov, Y. Yakovlev, A. Astrelin, S. Milligan and J. Palmateer, Volumetric performance evaluation of a laser scanner based on geometric error model, *Precis. Eng.* 40 (2015), 139–150.
- [22] Bala Muralikrishnan, Katharine M. Shilling, Daniel S. Sawyer, Prem K. Rachakonda, Vincent D. Lee, Steven D. Phillips, Geraldine S. Cheok and Kamel S. Saidi, Laser scanner two-face errors on spherical targets, in: *Proceedings of the Annual Meeting of the ASPE 2014*, 2014.
- [23] A. Nothnagel, M. Eichborn and C. Holst, Improved focal length results of the Effelsberg 100 m radio telescope, in: *21st Meeting of the European VLBI Group for Geodesy and Astronomy (EVGA 2013)* (N. Zubko and M. Poutanen, eds.), pp. 55–60, Reports of the Finnish Geodetic Institute, Espoo, Finland, March 5–8 2013.
- [24] J. O. Ogundare, *Precision Surveying. The Principles and Geomatics Practice*, John Wiley & Sons, 2015.
- [25] Y. Reshetyuk, A unified approach to self-calibration of terrestrial laser scanners., *ISPRS J. Photogramm.* 65 (2010), 445–456.
- [26] P. Sarti, C. Abbondanza, L. Petrov and M. Negusini, Height bias and scale effect induced by antenna gravitational deformations in geodetic VLBI analysis, *J. Geod.* 85 (2011), 1–8.
- [27] Volker Schwieger, *Nicht-lineare Sensitivitätsanalyse gezeigt an Beispielen zu bewegten Objekten*, Ph.D. thesis, German Geodetic Commission (DGK), C, No. 581, 2005.
- [28] H. Wolf, *Ausgleichsrechnung. Formeln zur praktischen Anwendung*, Dümmler, Bonn, 1975.